European Review for Medical and Pharmacological Sciences 2023; 27: 11614-11634

A risk model based on the tumor microenvironment to predict survival and immunotherapy efficacy for ovarian cancer

Y.-R. WANG[1], W.-L. WU[2], X. CHENG[3], H.-X. GAO[4], W. LI[1], Z.-Y. LIU[1]

[1]Department of Gynecology and Obstetrics, Hua Zhong University of Science and Technology Union Shenzhen Hospital, Shenzhen, China
[2]School of Medicine, Graduate School of Hebei North University, Zhangjiakou, China
[3]Clinical Laboratory Center, Beijing Friendship Hospital, Capital Medical University, Beijing, China
[4]Department of Respiratory and Critical Care Medicine, The First Affiliated Hospital of Xi'an Jiao Tong University, Xi'an, China

Abstract. – OBJECTIVE: Based on the interactions between immune components in the tumor microenvironment and ovarian cancer (OC) cells, immunotherapies have been demonstrated to be effective in dramatically increasing survival rates. This study aimed to identify landmark genes, develop a prognostic risk model, and explore its relevance to the efficacy of immunotherapy.

MATERIALS AND METHODS: A risk model was built based on the immune- and stromal-related genes, which were extracted from the OC gene expression data of "The Cancer Genome Atlas" (TCGA) database. Survival analysis and receiver operating characteristic (ROC) analysis were then conducted through the model's risk score pattern, which was established depending on the TCGA training cohort and verified based on the internal TCGA cohort and external "Gene Expression Omnibus" (GEO) datasets. Furthermore, the immune-related characteristics and prognostic values of the risk model were evaluated.

RESULTS: The prognostic risk model for ovarian cancer demonstrated excellent performance in predicting survival rates, as validated in both the TCGA and GEO databases. The model showed significant associations with 17 functional immune cells, 17 immune checkpoints, PD-1, and several immune pathways, suggesting its potential to enhance the efficacy of immunotherapy in OC.

CONCLUSIONS: The risk model developed in this study has the potential to serve as a prognostic marker for OC, enabling the development of personalized immunotherapy protocols and providing a theoretical basis for novel combinations of immunotherapeutic approaches.

Key Words:
Risk model, Tumor microenvironment, Ovarian cancer, Prognosis, Immunotherapy.

Introduction

Ovarian cancer (OC) is a highly fatal gynecological oncological disorder, ranking as the fifth leading cause of cancer-related mortality among women in the United States (US)[1]. Additionally, OC holds the third position in terms of global prevalence among all gynecological malignancies[2]. The prognosis is generally unfavorable due to the absence of early warning symptoms, effective diagnostic markers, tumor heterogeneity, and high drug resistance during chemotherapy[3]. Despite its aggressive phenotype and complex pathophysiology, the molecular mechanisms underlying OC remain unclear. The primary treatment for OC typically involves cytoreductive surgery combined with adjuvant therapies such as antiangiogenic therapy, chemotherapy, poly-adenosine diphosphate ribose polymerase inhibitor (PARPi) treatment, and occasionally, growth factor signaling inhibitors[4]. However, the current therapeutic options for OC patients are inadequate, leading to high rates of recurrence[5]. Recent studies[6,7] on immunotherapy have shown promising immune-related indicators that could be utilized for early diagnosis and effective treatment of OC.

The tumor microenvironment (TME) is a highly intricate and adaptable system that interacts with tumor cells, affecting cancer growth, development, and progression[6]. Accumulating evidence suggests that the TME plays a crucial role in carcinogenesis and possesses numerous regulatory functions in tumor growth and metastasis[7]. Among the tumor-infiltrating immune cells (TIICs), tumor-infiltrating lymphocytes (TILs) have been extensively studied and have been shown to

Corresponding Author: Z.-Y. Liu, MD; e-mail: liuzengyou66@hotmail.com

impact the clinical outcomes[8] and prognosis of neoadjuvant chemotherapy in OC[9], as tumor progression is regulated at the interface of TILs and cancer cells[10]. Multiple analyses of targeted drugs have indicated that TILs could serve as therapeutic targets to enhance the clinical efficacy of drugs. Recently, drugs targeting immune checkpoints have demonstrated significant improvements in survival for OC patients and have played pivotal roles in tumor immunotherapy[11]. However, OC exhibits limited activity with infrequent, durable responses to immunotherapy using immune checkpoint blockades (ICBs)[12]. Therefore, the development of new strategies to identify prognosis-related hallmarks and tumor-infiltrating immune cells, as well as enhance the efficiency of ICBs, holds promise for the management of OC. Our study aimed to systematically assess a predictive model about differentially expressed genes (DEGs), TIICs, immune signaling pathways, ICBs, and overall survival.

Materials and Methods

OC Datasets and Samples

The gene expression datasets and associated clinical annotations of OC cases were downloaded from "The Cancer Genome Atlas" (TCGA) database (https://portal.gdc.cancer.gov/) and "The Gene Expression Omnibus" (GEO) database (http://www.ncbi.nlm.nih.gov/geo/). Informed consent of the OC patients involved in this study was obtained from these public databases. A total of 379 RNA sequencing datasets [fragments per kilobase million (FPKM) value] of TCGA-OC specimens were procured from the Genomic Data Commons (GDC) website (https://portal.gdc.cancer.gov/), which was specifically used for integrative analysis[13]. Additionally, 260 GEO-OC samples were obtained from the GSE32062 DataSet of the GPL6480 platform (Agilent-014850 Whole Human Genome Microarray 4×44K)[14]. The inclusion criteria for the data were: (i) patients diagnosed with ovarian serous cystadenocarcinoma; (ii) datasets containing intact survival times and outcomes.

ImmuneScore and StromalScore Generation

The ESTIMATE algorithm used gene expression signatures to calculate the fraction of infiltrating immune and stromal cells for each sample in the TME in the form of ImmuneScore and StromalScore, respectively[15]. Furthermore, a total of 379 tumor specimens from TCGA were divided into two groups: (i) high and low ImmuneScore groups, and (ii) high and low StromalScore groups, based on their respective scores in relation to the median score. This categorization was performed to facilitate a comparison of the extent of immune-stromal component infiltration. Subsequently, the empirical Bayesian approach of the "limma" package in R investigated the gene expression variation between the high-scoring and low-scoring samples. The significance criteria for defining DEGs were set at an absolute value of logFC (fold change) greater than 1 and a false discovery rate (FDR) less than 0.05.

Weighted Gene Co-expression Network Analysis

Following data collection from TCGA, the expression profiles of the 379 OC samples were selected as an expression matrix to create a co-expression network using the WGCNA, a package in R[16]. Genes that lacked expression values were deleted while establishing the WGCNA network in this study. Initially, a hierarchical clustering tree was constructed utilizing gene interaction patterns, and significant outliers were removed. The optimal soft threshold was selected to create a closely scale-free co-expression network. Subsequently, the highly co-expressed gene modules were arranged into a hierarchical clustering tree by dividing different genes with comparable expression forms into the matching module. Based on the clinical information on immune and stromal scores, the correlations between clinical phenotype and gene modules were estimated to determine the most significant module. After acquiring the key gene module, the hub genes were detected by screening gene significance (GS) and module membership (MM) values. GS was the coefficient of connection between a specified gene's expression pattern and the module's corresponding phenotypic trait. The relationship coefficient between a module gene (the initial primary component of each module) and the gene expression level defined MM. This study evaluated genes with GS values greater than 0.50 and MM values greater than 0.60 as the modules' signature genes.

Identification of Simultaneously Expressed DEGs

Venn (https://bioinfogp.cnb.csic.es/tools/venny/index.html) is a collaborative online tool that

utilizes multiple established datasets to visually represent unions, intersections, and distinctions[17]. This study conducted an interaction analysis of hub genes derived from the key gene module and DEGs obtained from immune-stromal components to identify simultaneously expressed DEGs. Consequently, immune-related hub genes and stromal-related hub genes in OC patients were acquired.

Establishment and Validation of the Prognostic Risk Model

The union of the immune-related gene set was obtained and used for further analysis. Subsequently, the expression data (FPKM) and relevant clinical data of genes were extracted from TCGA-OC samples to assess the connection between hub genes and the overall survival rate for OC patients. All the clinical expression data of TCGA-OC samples were randomly categorized into a training group and authentication cohort in a ratio of 7:3, completing internal validation. In addition, data from the GEO database was used for external validation. The purpose of the training cohort was to establish a prognostic risk model, whereas the validation set was used to authenticate the model.

Univariate Cox Regression Analysis

A univariate Cox regression analysis was constructed in this research to identify potential risk factors and prognostic DEGs in hub genes found in the training group. The analysis was performed using the R package "survival" with the "Efron" method. A p-value < 0.05 was considered statistically significant for all the investigations.

Cox Regression Analysis with Multiple Variables

The prognostic genes obtained by univariate analysis were incorporated into a multivariate Cox regression analysis to develop a prognostic risk model. The multivariate Cox analysis used the stepwise regression analysis method to adjust the regression model and identify the optimal model in which the Akaike information criterion (AIC) was the smallest. Based on AIC statistics, the stepwise regression method deleted or added variables by selecting the smallest AIC values. Its primary function was to obtain the best regression equation for screening the genes associated with prognosis. This study measured these predictive gene risk scores through the linear part of the multivariate Cox regression model. The risk score calculation formula used for the evaluation is presented in Equation (1):

$$\text{Risk score} = \sum^{N} i = 1 \text{ Expi*Coei} \quad \text{Equation (1)}$$

where N is the gene number; Expi and Coei are the gene expression level and coefficient value, respectively[18]. Subsequently, the risk scores of individuals in the training group were calculated using the aforementioned formula. Patients in the training group were distributed into low-risk and high-risk clusters, with the cutoff value set to the medium-risk level, to evaluate the effect of prognostic genes obtained by multivariate analysis on the overall survival rate in OC. The "survminer" package (version 0.4.9) was employed to conduct survival analysis and visualizations.

Receiver Operating Characteristic Curve

A survival ROC analysis was conducted using the ROC package (version 1.0.3) to assess the effectiveness of the Cox hazards regression model. The ROC curve displayed the effect of grouping the model under all classification thresholds[19]. The false positive and true positive rates were plotted with respect to the graphical presentation of the ROC curve. The area under the ROC curve (AUC) is used as a summary value of prognostication of the ROC curve; the higher the AUC value, the better its prognostic accuracy. In the present study, the AUC values for the training cohort's 1-, 3-, and 5-year overall survival were estimated to measure the accuracy of the prognostic model. Risk score distribution plots, a heatmap of model gene expression, a survival curve comparing the high- and low risk groups, and ROC curves for individuals in the validation group were implemented to validate the model.

Analysis of Differences Between Low- and High-Risk Clusters

Analysis of immune cell differences in the training group

A single-sample gene set enrichment analysis (ssGSEA) was applied to reflect how the input gene checksum was coordinately upregulated or downregulated inside a sample[20]. This study used previously reported genes derived from multivariate Cox analyses and corresponding expression data to calculate the ssGSEA score for 29 immune cells of the immune microenvironment from 264 patients in the training cohort.

Investigation of Immune Checkpoint Differences of the Training Group

For the training group, the Wilcoxon test and the false discovery rate (method) were adjusted to identify the differentially expressed immune checkpoint molecules between the high-risk and low-risk categories based on immunological checkpoint molecular information. Given the extensive current research on programmed cell death 1 (PDCD1, also known as PD1, PD1 derived from the last step was selected as the target to search for its correlation with module genes of the risk model.

Verification of Immune Checkpoint Differences of the Validation Group

For the external verification group, the risk model was subsequently applied to the IMvigor210 cohort (http://research-pub.gene.com/IMvigor210CoreBiologies), a real immunotherapy cohort consisting of 298 RNA-seq datasets of metastatic urothelial carcinoma (mUC) patients who received PD-L1 blocking therapy[21], in order to assess the model's predictive capability for immunotherapy. Finally, the GSE32062 DataSet was utilized to evaluate the effectiveness of ICBs therapy by employing TIDE scores (available at https://tide.nki.nl)[22], which are based on the risk scores of the prognostic model. Notably, higher TIDE scores in this software indicate less effective the ICBs treatment (**Supplementary Table I**).

Gene Set Enrichment Analysis Between Low and High-Risk Categories

Gene expression changes among low and high-risk subtypes were examined by employing the "limma" package in R. The hallmark gene set was obtained from the Molecular Signatures Database (MSigDB). The c5.go.v7.4 and c2.cp.kegg collections were downloaded, including GO-BP, GO-MF, GO-CC, and KEGG. GSEA of the above DEGs was performed depending on the "Cluster Profiler" R set and the corresponding annotation gene sets.

Independent Prognostic Value of Risk Module

Univariate Cox regression analysis has shown the function of the aforementioned clinicopathological characteristics in forecasting the prognosis of risk models. This study assessed parameters such as stage, age, grade, race, tumor residual disease, and risk score. Parameters with a $p < 0.05$ were considered significant. To further validate the risk model and enhance its effectiveness, the factors with $p < 0.05$ were subsequently included in their models to construct a multivariate Cox regression analysis.

Creation of a Prognosis Nomogram for Survival Rate

Each parameter was assigned a score according to its role in the outcome variables of the nomograms. The total scores of all parameters were then converted into an estimate of the likelihood of outcome events[23]. In this study, a nomogram was developed, incorporating a risk score, to calculate the predictive values of 1-, 3-, and 5-year overall survival. The 1-, 3-, and 5-year survival calibration curves were plotted and utilized to calculate the prognostic accuracy of the above prognostic model. The closer the slope was to 1, the better its predictive accuracy.

Results

Study Procedure

A flow chart illustrating the data preparation, processing, and analysis in this study is shown in Figure 1. Data from the transcriptome and clinical data from 379 cases of TCGA were obtained to calculate the DEGs of stromal and immune elements in OC samples. ESTIMATE method was then employed to analyze the data. WGCNA was performed based on these phenotypes, and the key module trait and hub genes within the module were obtained. Finally, 312 DEGs related to the OC immune microenvironment were obtained to construct a prognostic prediction model for OC. A nine-gene model was created through multivariate and univariate Cox regression analysis. A risk score pattern was established depending on the expression levels of these nine genes in the TCGA training cohort. Based on the internal TCGA validating cohort and external GEO validating datasets, this study then focused on assessing the independent prognostic power of the risk model. Finally, the relevance of this risk model to immune cell differences, immune checkpoint differences between the high- and low-risk score, and the prognostic value of this model were investigated in particular.

StromalScore- and ImmuneScore-based DEGs

This study conducted a comparison between the low- and high-scoring categories to reveal 1,149 DEGs screened based on ImmuneScore.

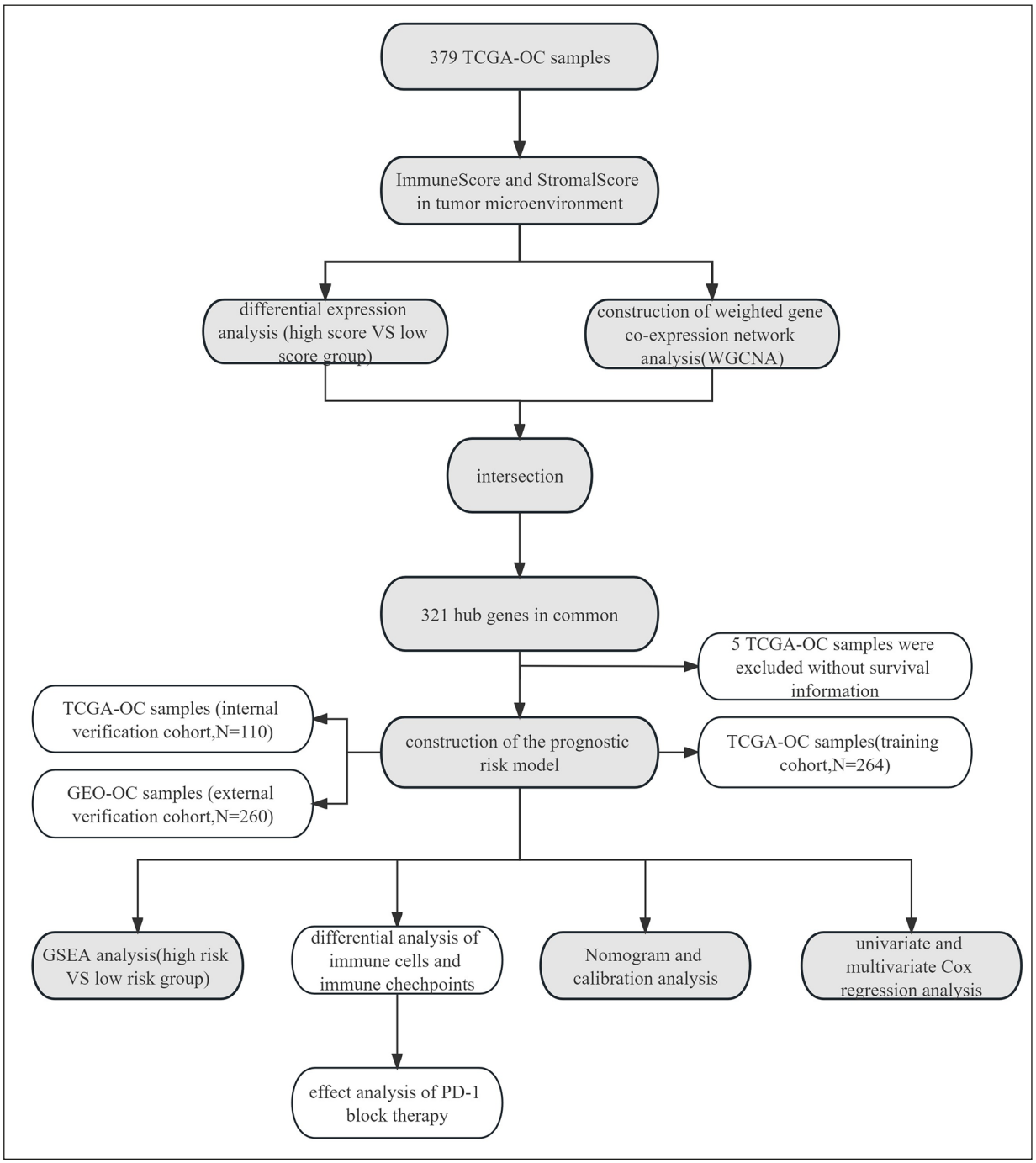

Figure 1. The overview of research design.

It included 629 upregulated and 520 downregulated genes. Similarly, 1,132 DEGs (734 upregulated genes and 398 downregulated genes) were acquired from StromalScore. The DEGs were visualized by volcano plots (Figures 2A and 2B) to understand the overall differential gene profile distribution. Heatmaps of the top 20 upregulated and downregulated DEGs in the immunological and stromal elements were also observed (Figures 2C and 2D).

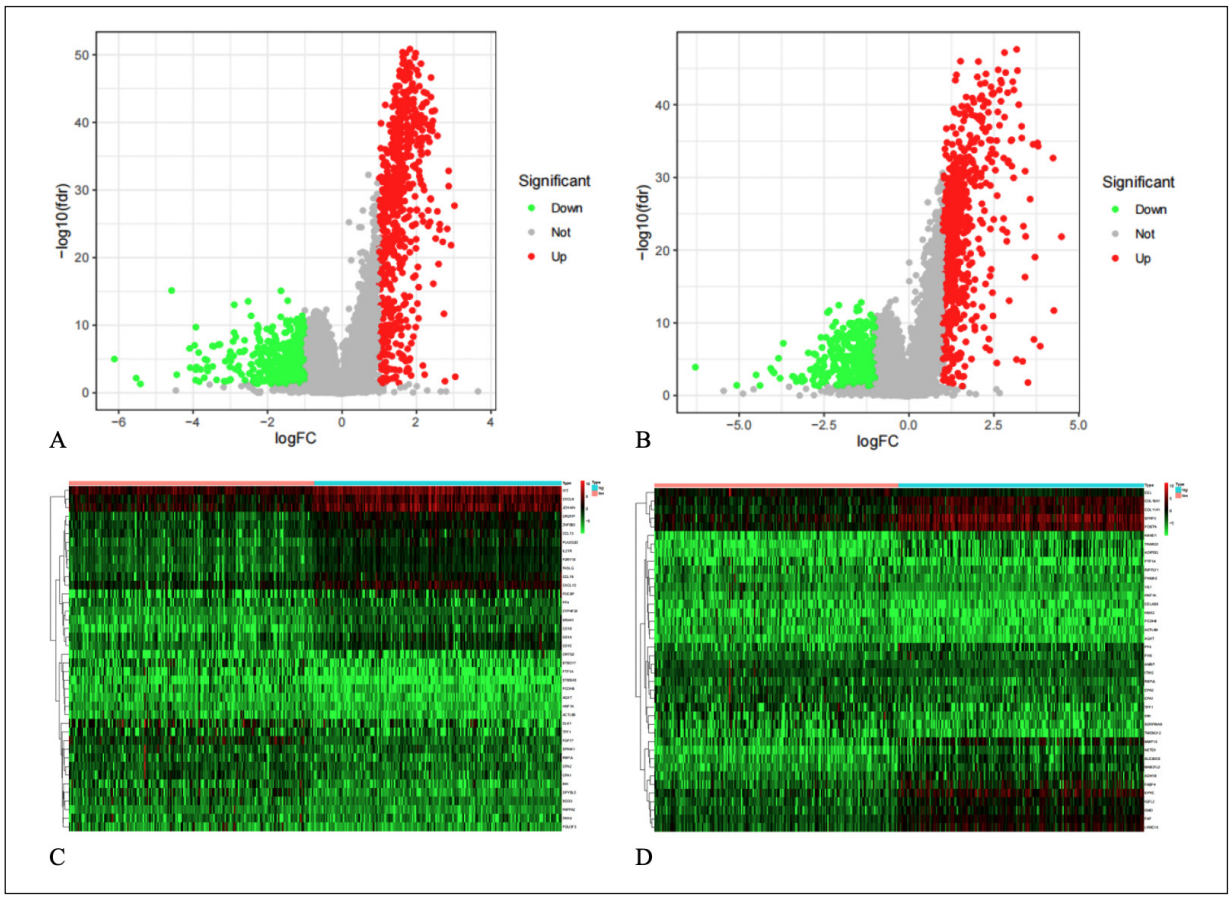

Figure 2. Volcano plots and heat maps of DEGs. **A-B**, Volcano plot of DEGs based on ImmuneScore and StromalScore, respectively. **C-D**, Heatmap of the top 20 DEGs based on ImmuneScore and StromalScore, respectively.

Construction of Weighted Gene Co-Expression Network Analysis

This study performed WGCNA (Figure 3) with the 379 identified OSC samples, forming a hierarchical cluster tree (Hclust value = 30,000, with four significant outliers removed) (Figure 3A). With a soft threshold power and a scale-free R^2 of 4 and 0.9, respectively, the gene distribution conformed to a scale-free topology model fit (Figure 3B). Hierarchical clustering results divided genes into WGCNA modules (Figure 3C). The module-trait relationships revealed that the module-trait "blue" was strongly linked with ImmuneScore (r = 0.58, p = 1e-35) and StromalScore (r = 0.9, p = 2e- 137). Therefore, the "blue" module was considered the key gene module. Setting GS > 0.5 and MM > 0.6 screened 357 hub genes in the ImmuneScore group (cor = 0.97, p < 1e-200) and 150 hub genes in the StromalScore group (cor = 0.85, p < 1e-200) from the "blue" module (Figures 3D and 3E).

Identification of Differentially Expressed Genes in Ovarian Cancer

This research performed an intersection analysis on the Venn plots of the DEGs in ImmuneScore, and the immune-regulated hub genes screened from the WGCNA identified 311 genes (Figure 4A). A total of 126 stromal-regulated genes were shared by stromal groups (Figure 4B).

Advancement and Validation of an Ovarian Cancer Prognostic Risk Model

Prognostic risk model and risk score assessment in a training cohort

This study obtained 312 DEGs from the union of the 311 immune-related genes and 126 stromal-associated genes identified above. According to the expression of DEGs and the corresponding survival information of 374 OC patients (excluding five samples without survival information) obtained from TCGA, 28 DEGs

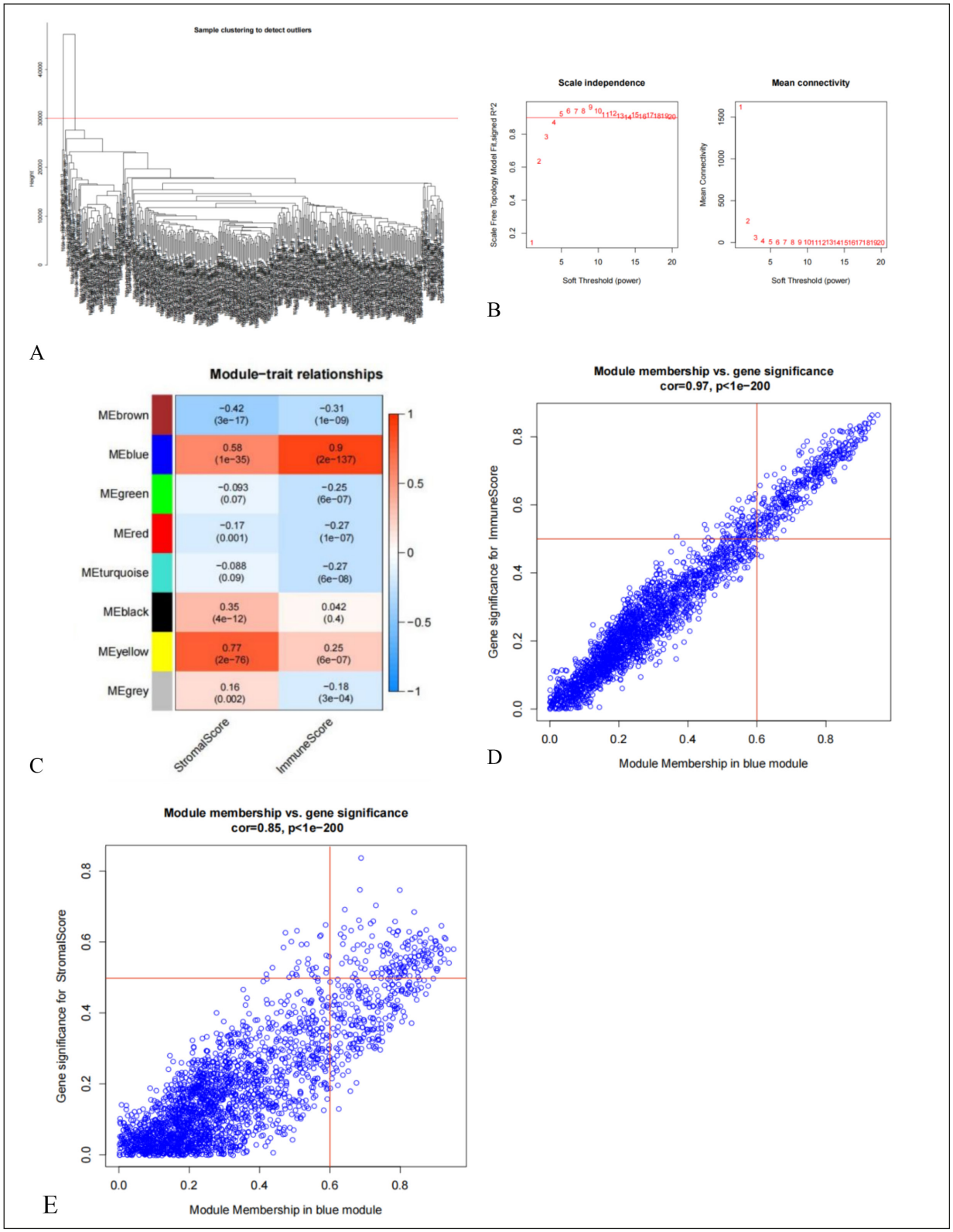

Figure 3. Results of the weighted gene co-expression network analysis (WGCNA). **A**, Hierarchical cluster tree with detected outliers. **B**, Network graph of all thresholds. **C**, Module-ImmuneScore/StromalScore correlations and the corresponding p-values. The color panel on the left displays eight modules, and the right scale shows module-trait relationships from –1 (*blue*) to 1 (*red*). **D-E**, Scatter plot representation of the correlation between gene significance for ImmuneScore and module "blue", and StromalScore and module "blue", respectively.

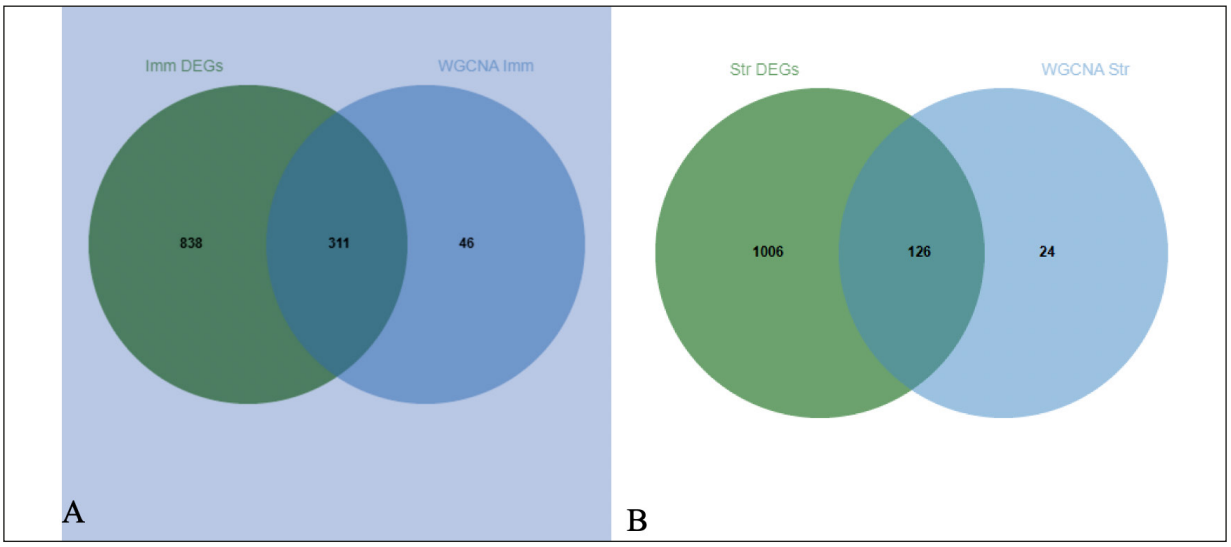

Figure 4. Venn diagrams showing common (**A**) immune-regulated and (**B**) stromal-regulated DEGs.

correlated with prognosis were identified through a univariate Cox regression analysis (Figure 5A). A successive deterioration method was applied using a multivariate Cox regression model for the above single prognostic factor analysis. An optimal model obtained nine prognostic genes (*GIMAP7, HTRA4, CCL5, ICOS, CD40LG, CD3G, VSIG4, CD2,* and *ANKRD22*). The risk score was generated using the linear part of the multivariate Cox regression model of these nine genes (Equation 2):

Risk score = (expression of *GIMAP7*) × (–0. 169715998) + (expression of *HTRA4*) × (– 1.744715582) + (expression of *CCL5*) × (–0.014980592) + (expression of *ICOS*) × (–0.806180272) + (expression of *CD40LG*) × (– 1.998681563) + (expression of *CD3G*) × (–0.841718491) + (expression of *VSIG4*) × (0.050245582) + (expression of *CD2*) × (0.433625656) + (expression of *ANKRD22*) × (–0.403295818)

Equation (2).

This study considered the risk score of every case in the training group, depending on the DEG appearance. Compared to the middle, individuals were categorized into high-risk (n = 132) and low-risk (n = 132) categories. The patient's risk curve (red for high-risk values and green for low-risk values) and the existing state diagram (green for alive, red for death) were mapped according to the risk model (Figures 5B and 5C). These risk graph results demonstrated that the greater the risk, the greater the fatalities.

Authentication of the prognostic risk model in a training cohort

The forecast model was validated, and the overall survival curve was plotted depending on the risk categories. The evidence showed that the high-risk category had a significant correlation with a poorer prognosis ($p < 0.05$) (Figure 5D). Survival analysis with an online tool, Gene Expression Profiling Interactive Analysis (GEPIA2), clarified the fundamental role of the nine genes in the overall survival of OC patients. Patients with higher expression levels of *CD2, HTRA4, ICOS, CD40LG,* and *CD3G* displayed better survival (**Supplementary Figure 1**). In contrast, the expressions of the other four signatures had no statistically significant relationship with overall survival. These outcomes were due to the bias of the research being based on single genes rather than multiple genes. Next, the ROC curve analysis was performed to calculate sensitivity and accuracy. The AUC values for the 1-year (0.728), 3-year (0.662), and 5-year (0.727) survival were treated as excellent for predictions (Figure 5E).

Authentication of the prognostic risk model in the validation cohort

This research sequentially plotted the risk curve (Figures 6A and 6B), the survival curve

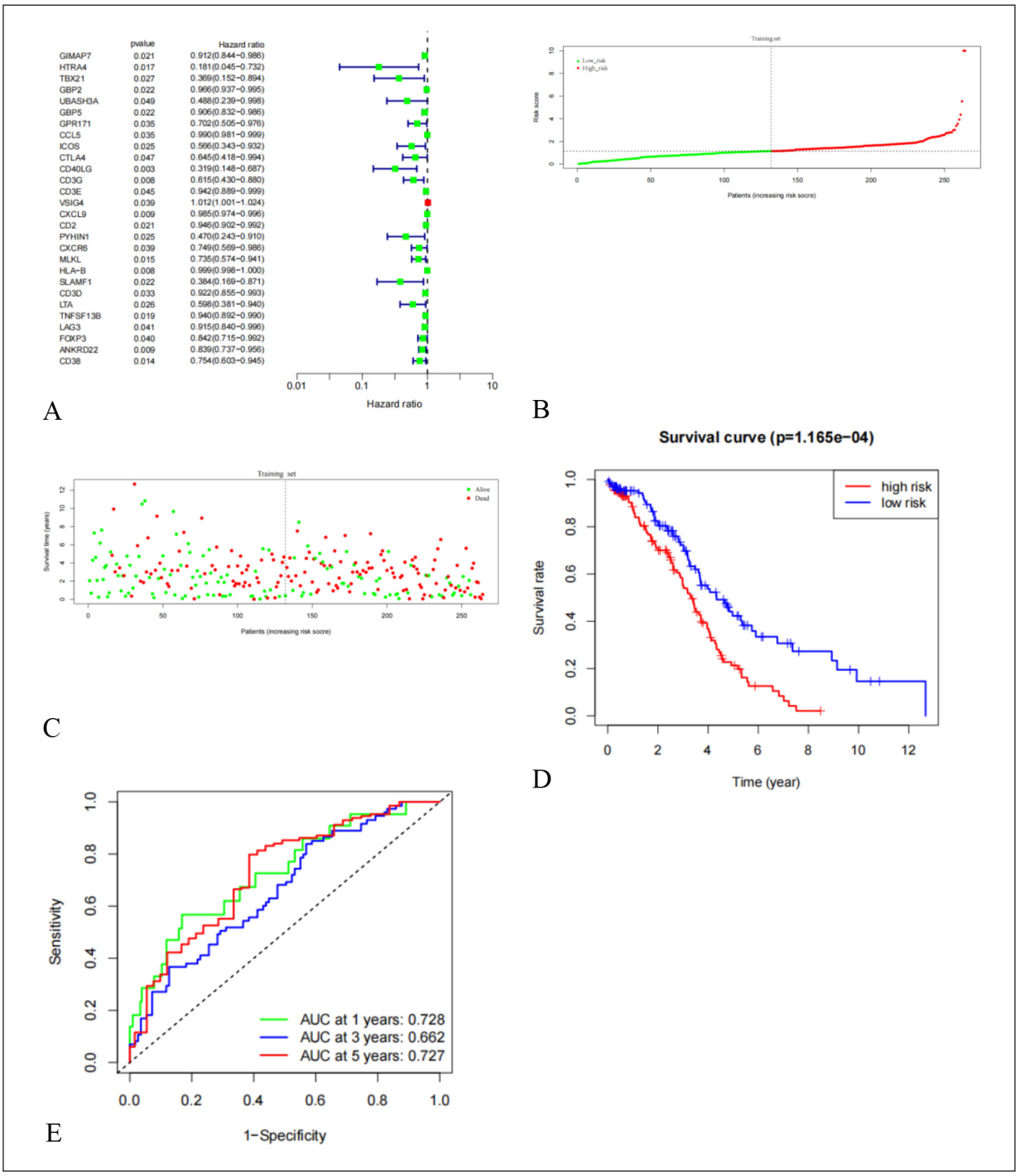

Figure 5. **A**, Univariate Cox regression analysis of the forest plot of prognostic DEGs for the training cohort. **B-C**, Risk score and survival state analyses between the high- and low-risk groups by signature. The x-axis and y-axis represent the rank of patients according to risk scores, and the risk score and survival time, respectively. The dotted line represents the median risk score and the corresponding number of patients. **D**, Kaplan-Meier analysis for OC patients between the high- and low-risk groups. **E**, ROC analysis of the risk model.

(Figure 6C), and the ROC curve (Figure 6D) for the internal validation of the TCGA data. The results also showed that the high-risk group had poorer survival rates, and the AUC values for 1-, 3- and 5-year survival were higher than 0.6 in the testing cohort. Likewise, the external verifi-

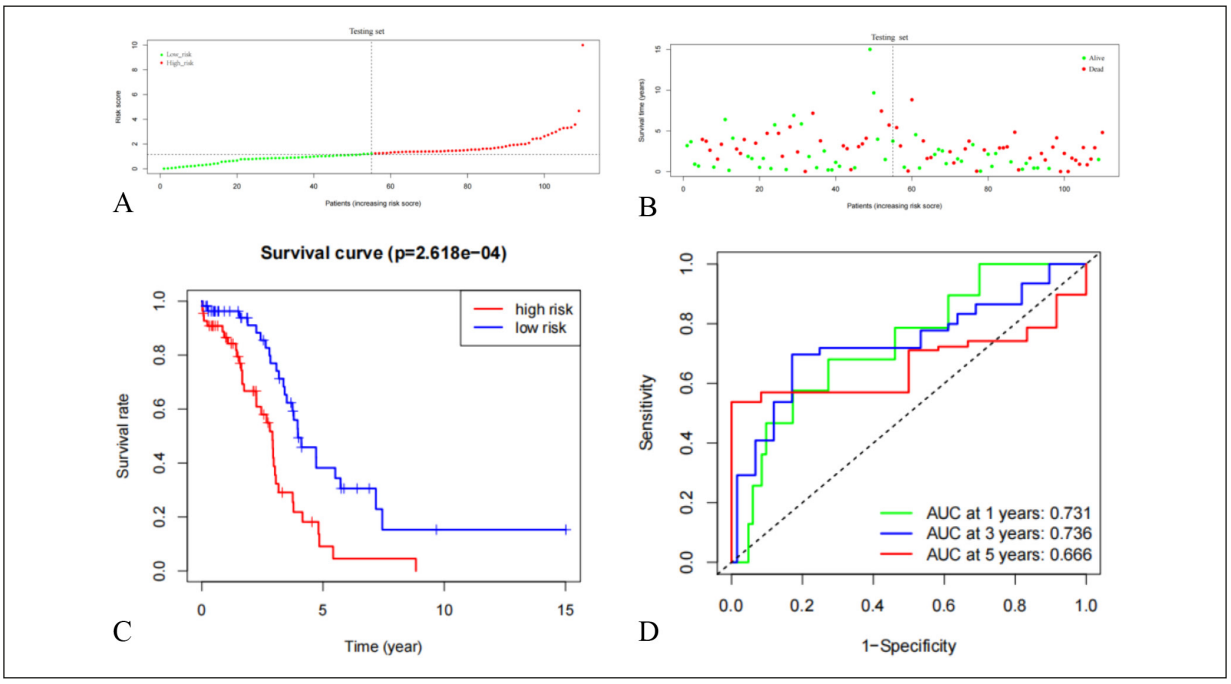

Figure 6. Analyses of the testing set. **A-B**, Risk score and survival state analyses between the high- and low-risk groups by signature. **C**, Kaplan-Meier analysis for OC patients between the high- and low-risk groups. **D**, ROC analysis of the risk model.

cation through GSE32062 DataSet demonstrated that similar results as the internal TCGA verification, confirming the robustness of the model (Figures 7A-D).

Tumor Microenvironment-Related Study

Investigation of immune cell differences

The ssGSEA was implemented to evaluate penetrating immunocytes to explore the differences in immune-related TME traits between the low and high-risk categories. The scores of 17 immune cells were significantly different, including Th 1 cells, follicular helper T (Tfh) cells, and inflammation-promoting cells (Figure 8).

Analysis of Immune Checkpoint Differences

The training cohort

The combination of risk score and immune checkpoint gene expression analysis showed that 17 genes were considerably different between the low- and high-risk categories (Figure 9). The correlation between the special immunological checkpoint molecule PD-1 and the nine model genes (Figure 10A-I) showed that PD-1 was positively associated with the nine hub genes of the training cohort ($p < 0.01$). Thereinto, the higher expression levels of *CCL5* (R = 0.74, $p <$ 2.2e-16) (Figure 10D), *CD2* (R = 0.79, $p <$ 2.2e-16) (Figure 10E), *CD3G* (R = 0.72, $p <$ 2.2e-16) (Figure 10F), *ICOS* (R = 0.70, $p <$ 2.2e-16) (Figure 10G), *GIMAP7* (R = 0.67, $p <$ 2.2e-16) (Figure 10H), *ANKRD22* (R = 0.66, $p <$ 2.2e-16) (Figure 10I) were considered excellent correlations as R > 0.6. The exceptions were *CD40LG* (R = 0.58, $p <$ 2.2e-16) (Figure 10A), *HTRA4* (R = 0.55, $p <$ 2.2e-16) (Figure 10B), and *VSIG4* (R = 0.34, $p <$ 6.8e-12) (Figure 10C) because their R-value was relatively low.

The external validation cohort

Through the risk assessment of 298 mUC samples of IMvigor210 based on the risk model established in this paper, 43 patients who exhibited a partial response (PR) to anti-PD-1 antibodies had a statistically higher risk score compared to the 25 patients who showed a complete response (CR) (p = 0.041) (Figure 11A). This finding suggests that a higher risk score, as determined by the prognostic model, is associated with a poorer therapeutic response to anti-PD-1 antibodies. In terms of the GSE32062 samples of GEO, Spearman's correlation test found that the risk score is significantly positively correlated with TIDE scores (cor = 0.46, p = 2.93e- 12) (Figure 11B), that is to say, the risk score is ne-

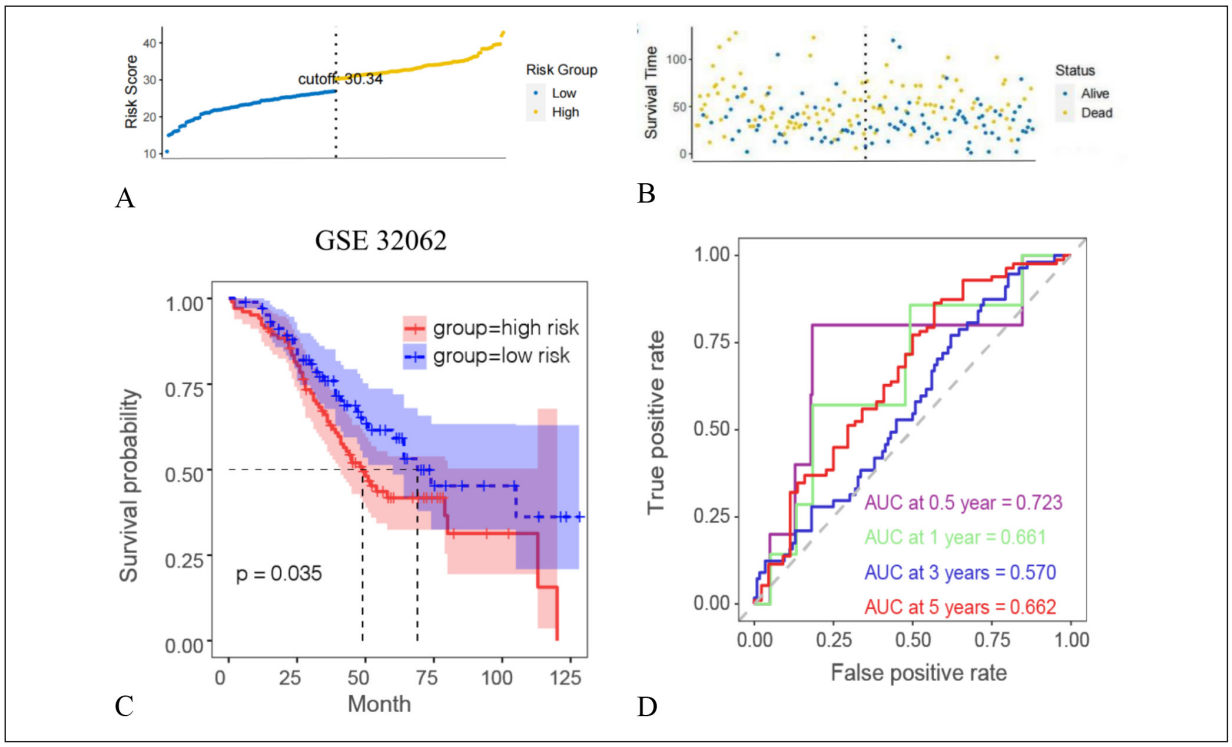

Figure 7. Analyses of external validation of the GEO-OC data. **A-B**, The plot exhibit the risk score and survival state analysis between the high- and low-risk group by signature, (**C**) Kaplan-Meier analysis between the high- and low-risk groups, and (**D**) ROC analysis of this risk model.

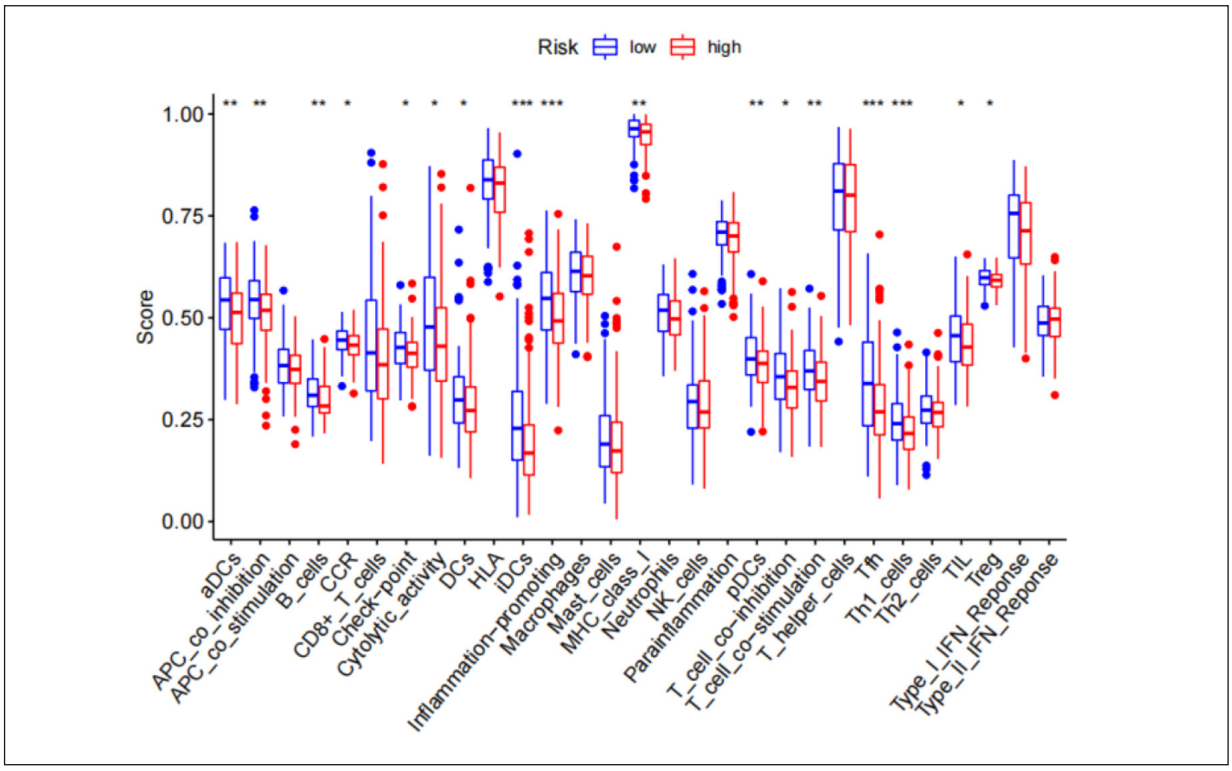

Figure 8. Analyses about immune cells differences between the high- and low-risk groups of the training set.

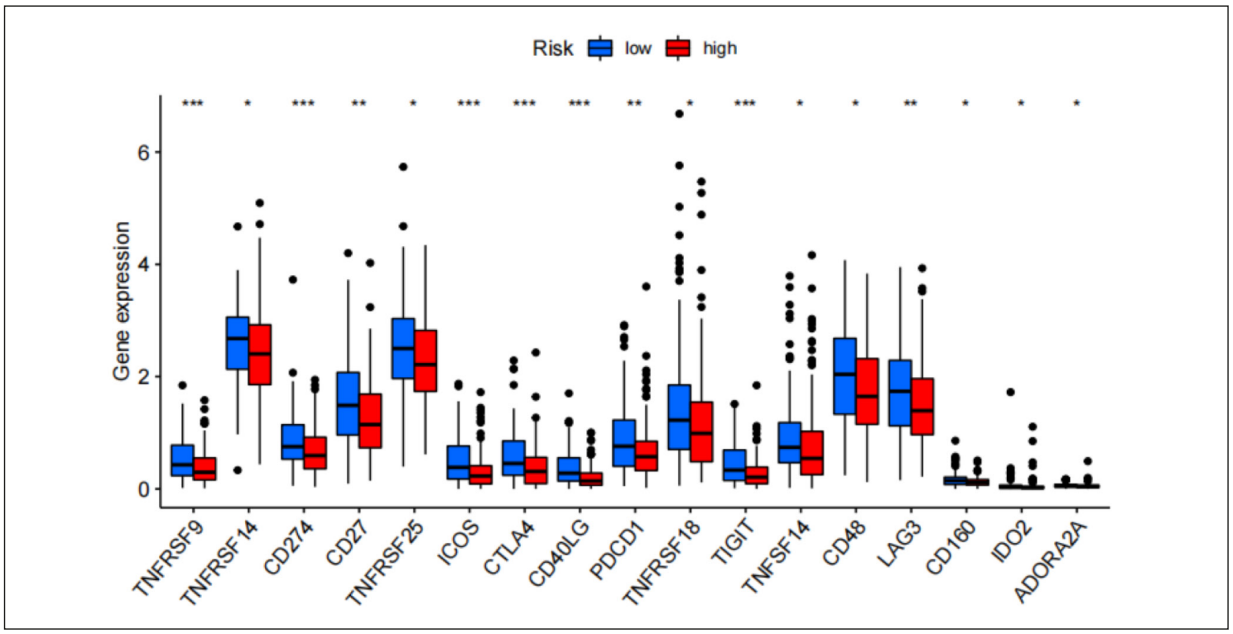

Figure 9. Analyses about immune checkpoint molecules differences between the high- and low-risk groups of the training set.

gatively related with the efficacy of ICBs therapy. At the same time, 68.00% (102/150) of the ICB-effective group and only 3.45% (2/58) of the ICB-ineffective group were in the low-risk set (p = 2.51e-16) (Figure 11C). The verification result of the GEO is consistent with the results of IMvigor210.

Gene set enrichment analysis enrichment analysis

GSEA analysis was carried out using the "Cluster Profiler" R package to compare the low-risk and high-risk clusters with the average risk score, as the risk score was found to be associated with the survival of OC patients. In the low-risk group, the DEGs were found to be enriched in several immune-related processes (Figure 12A), including autoimmune thyroid disease, antigen processing and presentation, the intestinal immune network, and IGA production. However, the DEGs were enriched in only one pathway for the high-risk group (not displayed). When considering the collection defined by MSigDB, the DEGs in the low-risk group were mainly enriched in various immune cell events, including adaptive immune response, positive regulation of the immune response, and regulation of T cell activation (Figure 12B). In the high-risk group, the genes improved mRNA translation and protein synthesis (Figure 12C). These outcomes suggested that the risk model may serve as a potential indicator of the TME status in OC patients.

Assessment of the Independent Prognostic Power of the Risk Model

To investigate the relationship between prognosis and clinical and pathological features of OC patients, age, race, tumor stage, tumor grade, residual tumor disease, and risk score in the predictive risk model were included in the univariate Cox regression analysis. The outcomes showed that only the p-values of residual tumor disease and the risk score were lower than 0.05 (Figure 13A). Consequently, these two clinical factors were incorporated into the multivariate Cox regression analysis. The p-value of the risk score was identified as having prognostic significance (Figure 13B). Therefore, the prognostic value of the risk score was unaffected by other clinicopathological features.

Nomogram Construction for Survival Prediction

According to the total scores, this study constructed a prognostic nomogram with risk scores to predict the 1-, 3-, and 5-year overall survival. The greater the score, the lower the overall survival rate (Figure 14A). Calibration curves were plotted to predict OC patient survival probabilities at 1-, 3-, and 5-year in the training group

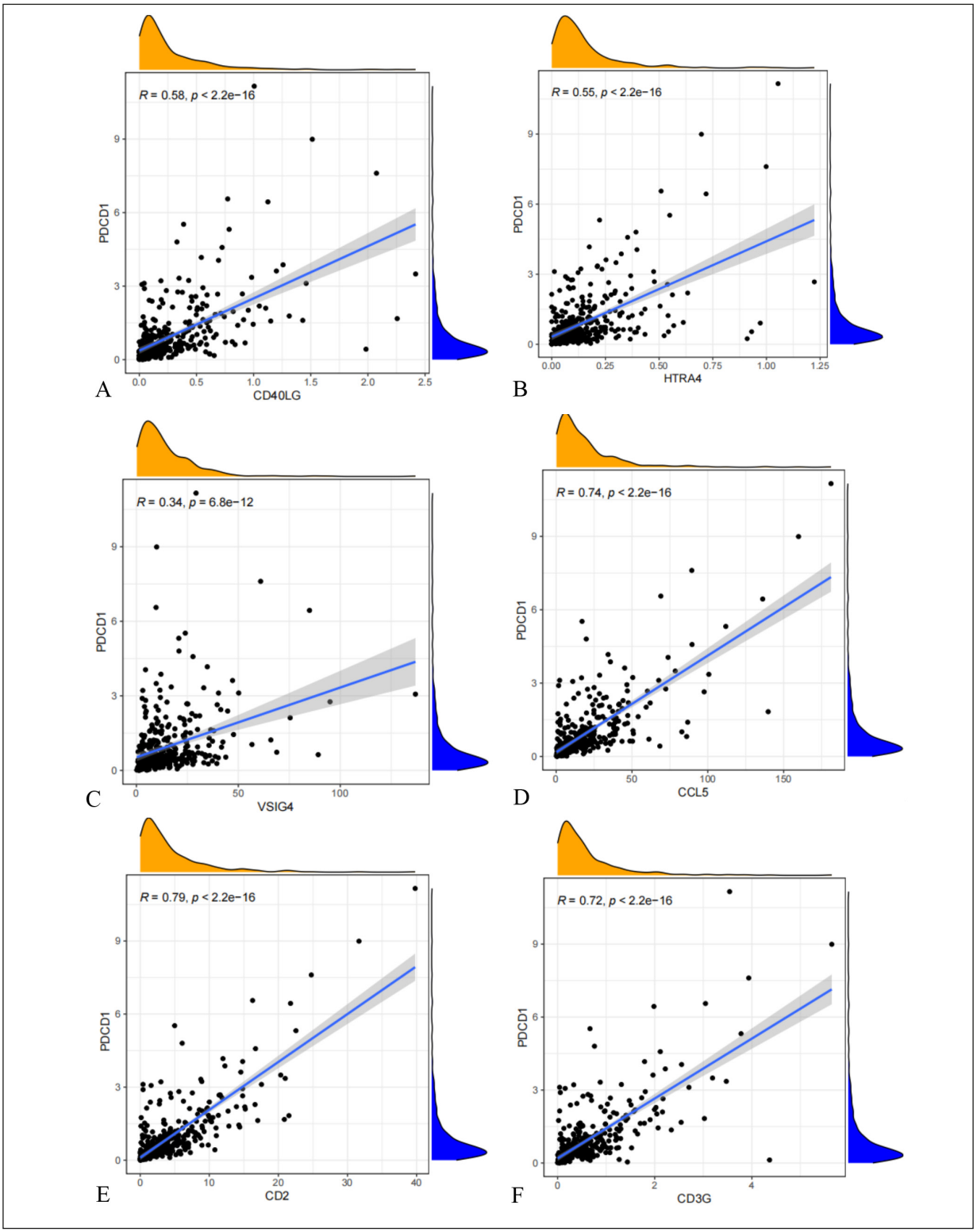

Figure 10. A-I, Scatter plots showing the correlation of PD-1 with the expressions of the nine genes using the Pearson coefficient. The blue line in each plot is a fitted linear model indicating the level of PD-1 along with model gene expression.

Continued

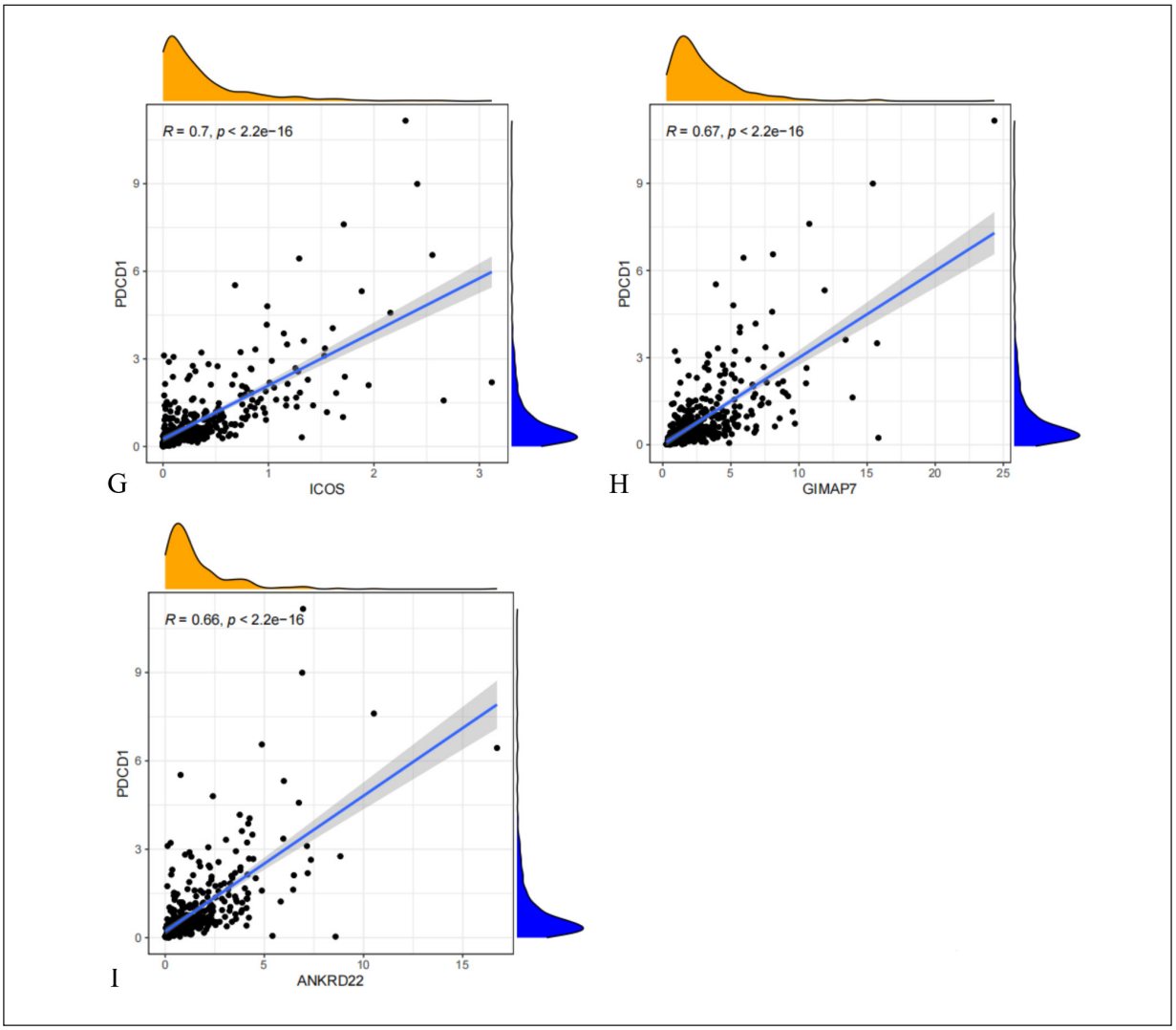

Figure 10 ***(Continued).*** **A-I**, Scatter plots showing the correlation of PD-1 with the expressions of the nine genes using the Pearson coefficient. The blue line in each plot is a fitted linear model indicating the level of PD-1 along with model gene expression.

(Figures 14B, 14C, and 14D). The closer the slope was to 1, the higher the prediction accuracy. The results of forecasting the 1-, 3- and 5-year overall survival showed that the model's accuracy in forecasting prognosis was very high, indicating that the prediction model was valid.

Discussion

OC patients experience poor prognoses, and researchers have developed prognostic models to ameliorate this condition. The use of risk models to predict the survival of OC patients dates back to 1,998, although only 40 patients were included[24]. An integrated clinical-and-gene model, which was assumed to be superior to the clinical-alone model, was constructed in 2,016 based on mRNA and microRNA expression profiles from TCGA[25]. Wang et al[26] also stressed the importance of developing predictive markers for OC. Therefore, this study aimed to develop a new, effective, and accurate gene risk prediction model.

OC is tumor immunogenicity, and TME is a complex network composed of immune cells, stromal cells, cancer cells, and the surrounding signal molecules. It is critical for tumorigenesis and development. Evidence shows that TILs play an active role in clearing ovarian tumors and improving clinical outcomes by recognizing tumor

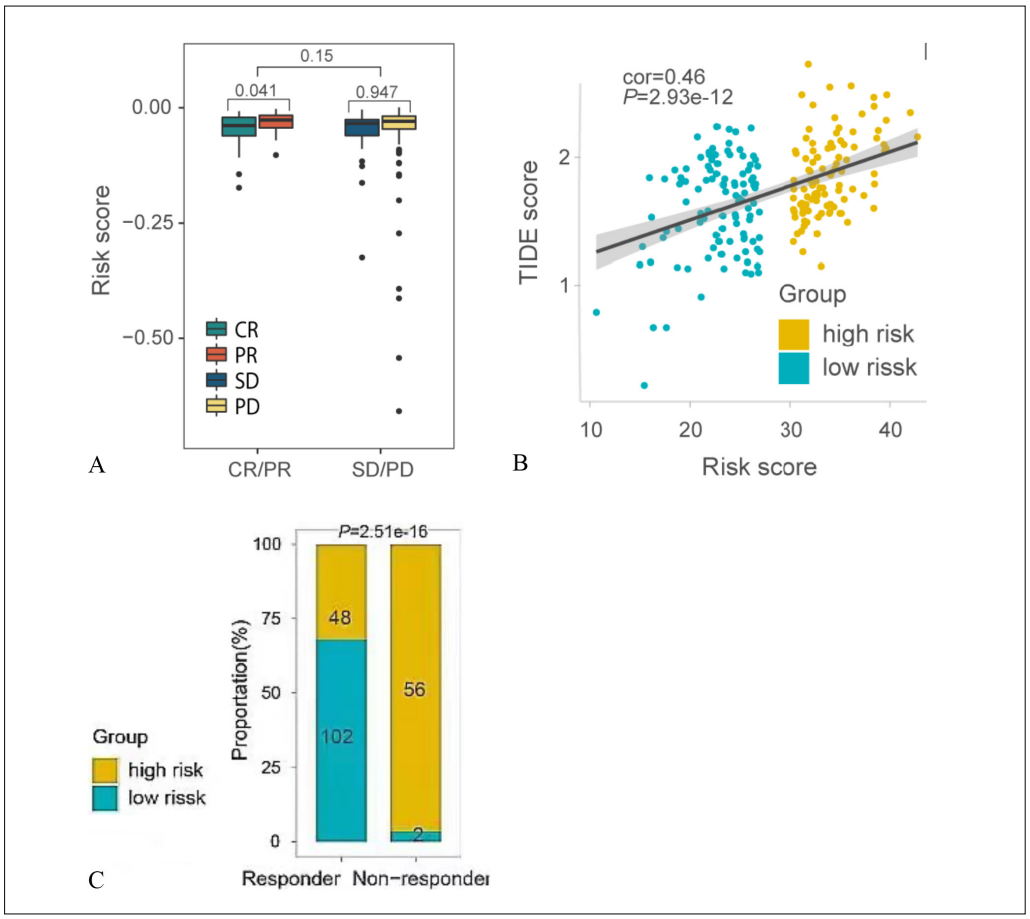

Figure 11. A, External Validation of IMvigor210. The risk score differences between groups with different reactions to anti-PD-1 antibodies. PD: progressive diseases (n = 167), SD: stable disease (greater than 6 months, n = 63), PR: partial response (n = 43), CR: complete response (n = 25). External Validation of GSE32062 was exhibited by (**B**) and (**C**): (**B**) is the relationship between the risk score and the TIDE score and (**C**) is the relationship between the risk score and the respond rate to ICB.

antigens and secreting cytokines characteristic of effector cells[27]. Stromal components suppressed the antitumoral immune response in some cases. Yang et al[28] reported high immunological and stromal scores related to lymphatic and venous invasion in OC and higher stromal and lower immune scores for healthy cells. These findings illustrated that the role of stromal and immune cells in patient prognosis in OC is distinct and complicated at different stages.

Therefore, this study developed a nine-gene predictive model with significant association with overall survival based on the close correlation between the immune system and patient outcomes in OC, indicating that immune and stromal cells had a vital function in diagnosing OC. Other studies[31] showed good overall survival rates in gastric cancer[29] and lung adenocarcinoma[30], associated with greater stromal-immune scores, while low stromal scores were good factors in colon cancer patients. However, this study found that a reduced stromal-immune risk score was associated with a good survival rate in OC patients, indicating that stromal-immune scores might play distinct roles in the prognosis of different tumors. Based on the results, the prognosis-related model might significantly change immunotherapeutic effects, influenced by the heterogeneity in OC, and provide potential guidance for prognostic stratification.

In the risk score formula, overexpression of *VSIG4* and *CD2* had a positive and significant effect, demonstrating that these could increase the risk score and were associated with a poor prognosis. Seven genes (*GIMAP7, HTRA4, CCL5, ICOS, CD40LG, CD3G,* and *ANKRD22*) had a negative coefficient, contributing to improved overall survival. *VSIG4*, a new macrophage protein

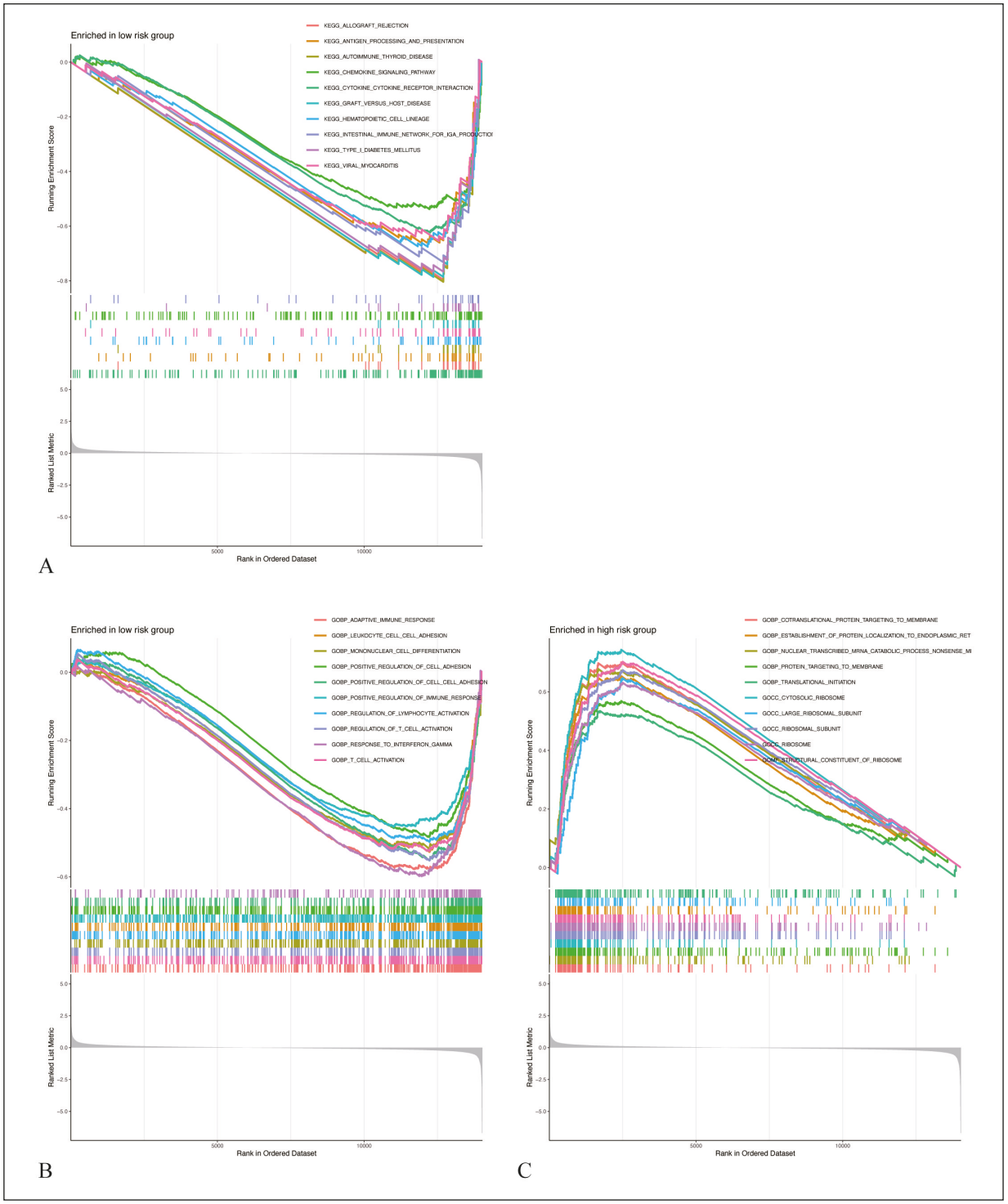

Figure 12. GSEA of samples with high- and low-risk groups. **A**, The top 10 enriched KEGG pathways of the low-risk group. Each line represents one pathway with a unique color Positively correlated pathways are located above the x-axis, while negatively correlated pathways are below the x-axis. **B**, The top 10 enriched GO terms in the low-risk group. **C**, The top 10 enriched GO terms in the high-risk group.

from the B7 family, suppressed T-cell activation and promoted OC growth[32]. Multiple studies[33] about solid tumors have confirmed that *CD2* is associated with prognosis. *CD2* is correlated with a better prognosis in breast carcinoma and participates in tumor invasion. For ovarian, endometrial,

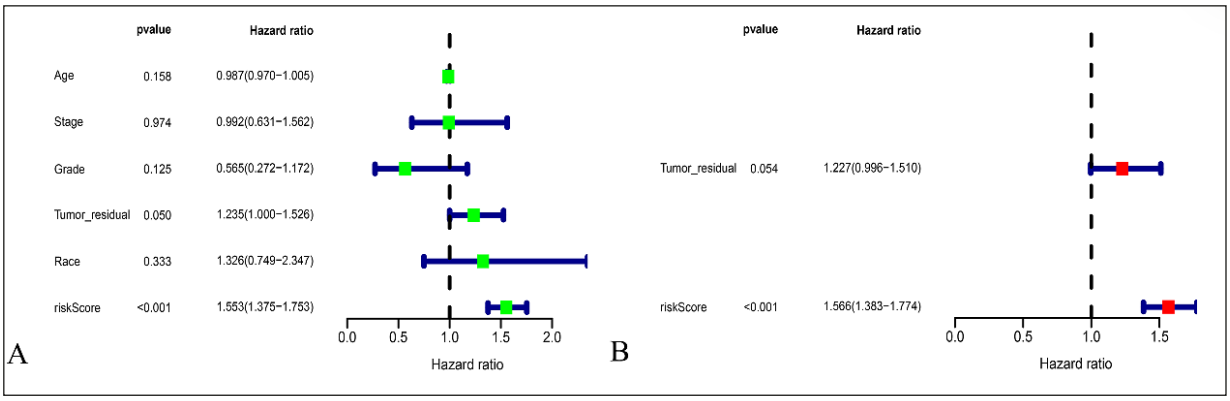

Figure 13. **A**, Univariate and (**B**) multivariate Cox prognostic analyses of the training cohort.

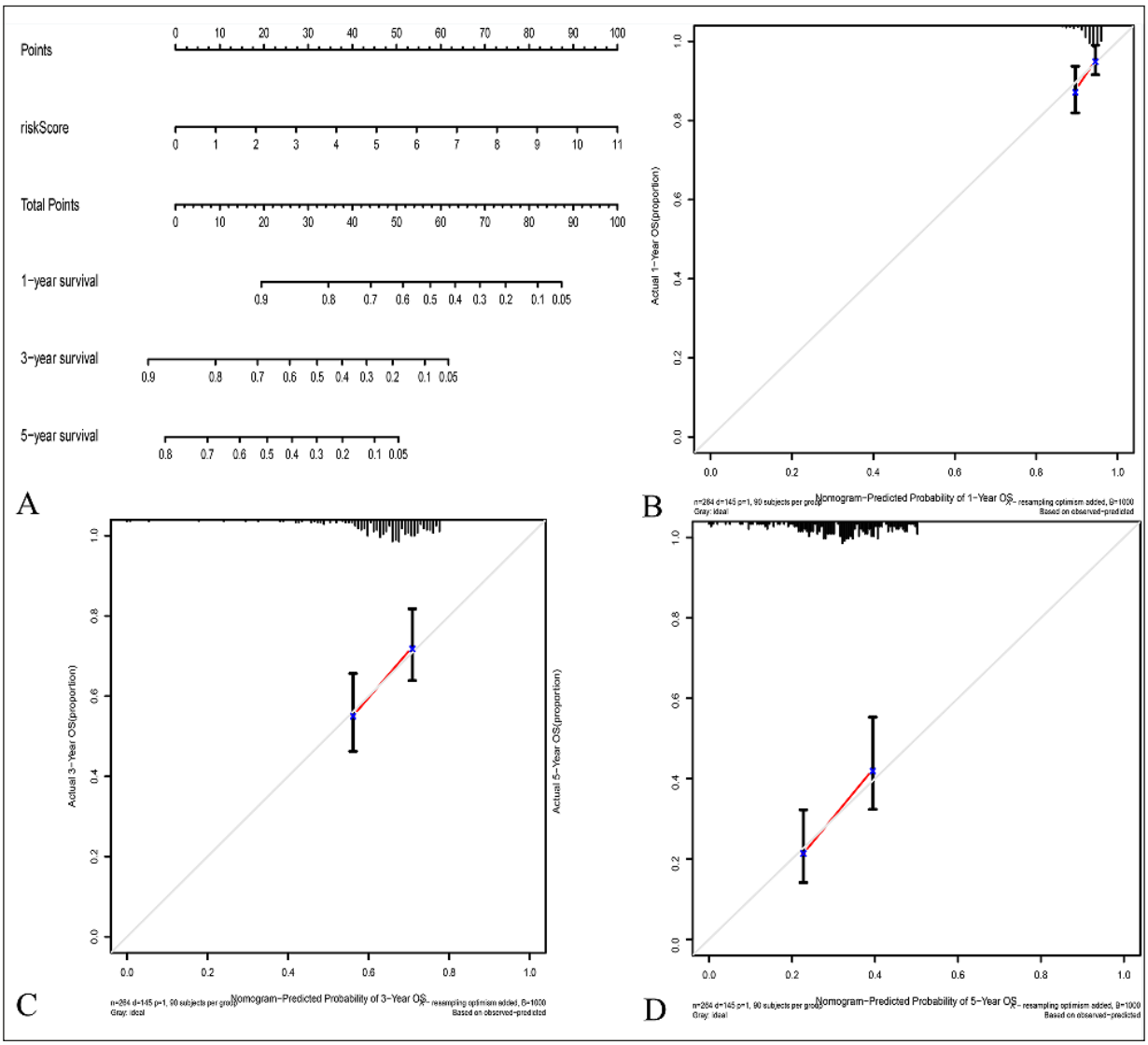

Figure 14. Nomogram of 1-, 3-, and 5-year overall survival (**A-D**) Calibrations of 1-, 3-, and 5-year overall survival.

and colorectal malignancies, the downregulation of *CD2* weakens PD-1 immunotherapy efficacy by reducing antitumor T-cell responses[34]. Researchers have reported that *CD2* plays a role in T, natural killer (NK) cell activation, and signaling pathways in immunoregulation[35]. However, this paper found that *CD2* was related to increased risk scores and contributed to a poor prognosis, suggesting that *CD2* might be the biological hallmark of tumor survival. *GIMAP7* predicts better survival status in most tumor types[36], agreeing with this study's finding. Schwefel et al[37] found that *GIMAP7* directly impacted survival and homeostasis regulations, and it was positively related to the high quantity of CD8+ and CD4+ T cells in the TME. *HTRA4* is an apoptosis regulator that increases cell cycle arrest in the G2/M phase, stimulates cell death, and participates in oncogenesis in brain, breast, and prostate tumors[38].

Several researchers[39] have reported that *CCL5* modulates immune cell infiltration (NK cells and T cells) in solid cancers. Therefore, *CCL5* might be a perfect target for predicting OC cell survival. Similar to previous work[40], this study found that *CCL5* was a good signature to the high overall OC patient survival. *ICOS* was found to be highly correlated with an enhanced total life cycle in the TCGA ovarian tumor cohort. High-grade serous ovarian cancer (HGSOC) has demonstrated the pro-apoptotic effects of *CD40LG*[41]. *CD3G*, whose defect is associated with T-cell immunodeficiency[42], has been proposed as a novel biomarker for tumor development through its modulation of the T-cell receptor complex (TCR) signaling pathway[43]. For lung cancer, *ANKRD22* promotes cell propagation by increasing the expression of *E2F1* and facilitating cell cycle progression[44]. In contrast, *ANKRD22* is a tumor suppressor in prostate cancer[45]. *ANKRD22* can play a beneficial or detrimental role in the tumor context, and its effects on the tumorigenesis of OC need to be investigated. This study found that the oncogenesis and prognosis of OC involve multiple TME signatures, providing new insights into immunotherapy protocols for OC.

Furthermore, this study conducted ssGSEA and found that 17 functional immune cells were associated with risk score changes, indicating that specific immune cells in TME affected the risk score and prognosis of OC. It was found that the accumulation of these immune cells, such as Tfhs, TILs, and regulatory T cells (Tregs), increased in patients with lower risk scores. Studies[46] have indicated that TILs, which include macrophages, T cells, B cells, and NK cells, play a vital role in controlling solid tumor growth. For ovarian cancer, the TILs infiltration is prognostic for increased overall survival, while increased immunosuppressive Tregs are related to poor outcomes. Antigen-presenting cells (APCs) mainly comprise dendritic cells (DCs), macrophages, and B cells. Depending on the targeted cell types, APCs can be defined by their different abilities to capture, process, and present exogenous antigens to T-cells. As for solid tumor regions, DCs are considered the dominant cell populations for tumor antigen uptake and presentation. Similar to APCs, DCs initiate antitumor T-cell activation by transmitting tumor antigens to the draining lymph nodes, bridging the gap between innate and adaptive immunity, and regulating immunotherapy outcomes within tumors[47]. This study theoretically indicated that the risk score-based predictive model might be a useful biomarker for OC therapy. It could enhance the immunogenicity of cancer and chemo-preventive immune responses[33].

This study identified immune checkpoint molecules as important regulatory factors of the antitumor immune response. ICBs could block the immune escape of the tumor and reactivate the immunological system by eliminating critical targets in the tumor immune tolerance process[48]. Surprisingly, 17 immune checkpoint molecules were closely related to the predictive model in terms of differential expression. This observation indicated that ICBs could foster clinical success. As a most widely used ICBs, anti-PD-1 therapy has yielded encouraging results in OC patients[49]. Some researchers[50] suggest that inhibiting indoleamine-2, 3-dioxygenase1 (IDO1) in tumor-repopulating cells (TRCs) could pave the way for the development of future PD-1-targeting drugs. Preclinical experiments in murine OC models showed that combining PARP inhibitors and PD-1 blockades could lead to significant effects in OC[51]. This study's differential analysis demonstrated prominent interactions between the level of PD-1 and the nine genes of the predictive model. This result enabled a better understanding of PD-1 therapy in OC immunology and might constitute a new drug development method for targeting PD-1 expression.

GSEA elucidated biological functions to analyze the correlation between the values of the predictive model and the immune microenvironment. This study's results suggested that immune processes were significantly improved in the low-risk score group. These processes included antigen

presentation and processing, cytokine-cytokine receptor relations, and chemokine signaling pathways. Similarly, GO items, corresponding to active immune responses, were more prevalent in low-risk OC patients. These items included T-cell activation, lymphocyte activation, adaptive immune response, leukocyte cell-cell adhesion, positive cell adhesion regulation, and positive immune response regulation. However, there were no immune-related signaling pathways and GO items in the high-risk score set. The findings in the low-risk score group were consistent with the currently accepted view that activating specific immune responses plays a facilitating role in suppressing malignant progression and death. Therefore, this study confirmed that a forecasting framework based on risk score could be used as a suitable biomarker for tumor immunotherapy because of its robustness and good applicability in clinical practice.

Limitations

This study has some limitations. Despite internal validation and the nomogram, the statistical bias of the risk model could not be avoided completely without external validation datasets. TCGA-OC and ICGC-OC datasets, bioinformatics analysis, and qRT-PCR analysis confirmed the predictive value of the risk model. However, additional experimental validation, such as immunohistochemistry (IHC) assays and western blotting analysis, is essential to validate these findings prospectively.

Conclusions

In summary, we have successfully developed a prognostic signature comprising nine genes that exhibit robust predictive value. This study significantly enhances the effectiveness of immunotherapy treatment for patients with ovarian cancer (OC).

Conflict of Interest

The authors declare that they have no conflict of interests.

Ethics Approval and Informed Consent

Not applicable.

Funding

This research received no funding.

Authors' Contribution

Conceptualization, Yaru Wang; methodology, Yaru Wang and Wenlong Wu; Software, Xin Cheng; validation, Hengxing Gao and Wan Li; formal analysis, Yaru Wang and Wenlong Wu; data curation, Wan Li; writing-original draft preparation, Yaru Wang; writing-review and editing, Wenlong Wu and Xin Cheng; visualization, Hengxing Gao; supervision, Zengyou Liu. All authors have read and agreed to the published version of the manuscript.

References

1) Siegel RL, Miller KD, Jemal A. Cancer statistics, 2019. CA Cancer J Clin 2019; 69: 7-34.
2) Cabasag CJ, Arnold M, Butler J, Inoue M, Trabert B, Webb PM, Bray F, Soerjomataram I. The influence of birth cohort and calendar period on global trends in ovarian cancer incidence. Int J Cancer 2020; 146: 749-758.
3) Al-Alem LF, Pandya UM, Baker AT, Bellio C, Zarrella BD, Clark J, DiGloria CM, Rueda BR. Ovarian cancer stem cells: What progress have we made? Int J Biochem Cell Biol 2019; 107: 92-103.
4) Cortez AJ, Tudrej P, Kujawa KA, Lisowska KM. Advances in ovarian cancer therapy. Cancer Chemother Pharmacol 2018; 81: 17-38.
5) Kuroki L, Guntupalli SR. Treatment of epithelial ovarian cancer. BMJ 2020; 371: m3773.
6) Ni Y, Soliman A, Joehlin-Price A, Abdul-Karim F, Rose PG, Mahdi H. Immune cells and signatures characterize tumor microenvironment and predict outcome in ovarian and endometrial cancers. Immunotherapy 2021; 13: 1179-1192.
7) Hinshaw DC, Shevde LA. The tumor microenvironment innately modulates cancer progression. Cancer Res 2019; 79: 4557-4566.
8) Heindl A, Khan AM, Rodrigues DN, Eason K, Sadanandam A, Orbegoso C, Punta M, Sottoriva A, Lise S, Banerjee S, Yuan Y. Microenvironmental niche divergence shapes BRCA1-dysregulated ovarian cancer morphological plasticity. Nat Commun 2018; 9: 3917.
9) Khairallah AS, Genestie C, Auguste A, Leary A. Impact of neoadjuvant chemotherapy on the immune microenvironment in advanced epithelial ovarian cancer: prognostic and therapeutic implications. Int J Cancer 2018; 143: 8-15.
10) Zhang AW, McPherson A, Milne K, Kroeger DR, Hamilton PT, Miranda A, Funnell T, Little N, de Souza CPE, Laan S, LeDoux S, Cochrane DR, Lim JLP, Yang W, Roth A, Smith MA, Ho J, Tse K, Zeng T, Shlafman I, Mayo MR, Moore R, Failmezger H, Heindl A, Wang YK, Bashashati A, Grewal DS, Brown SD, Lai D, Wan ANC, Nielsen CB, Huebner C, Tessier-Cloutier B, Anglesio MS, Bouchard-Côté A, Yuan Y, Wasserman WW, Gilks CB, Karnezis AN, Aparicio S, McAlpine JN, Huntsman DG, Holt RA, Nelson BH, Shah SP. Interfaces of malignant and immunologic clonal dy-

namics in ovarian cancer. Cell 2018; 173: 1755-1769.e22.

11) Shi Z, Zhao Q, Lv B, Qu X, Han X, Wang H, Qiu J, Hua K. Identification of biomarkers complementary to homologous recombination deficiency for improving the clinical outcome of ovarian serous cystadenocarcinoma. Clin Transl Med 2021; 11: e399.

12) Disis ML, Taylor MH, Kelly K, Beck JT, Gordon M, Moore KM, Patel MR, Chaves J, Park H, Mita AC, Hamilton EP, Annunziata CM, Grote HJ, von Heydebreck A, Grewal J, Chand V, Gulley JL. Efficacy and safety of avelumab for patients with recurrent or refractory ovarian cancer: phase 1b results from the JAVELIN solid tumor trial. JAMA Oncol 2019; 5: 393-401.

13) Colaprico A, Silva TC, Olsen C, Garofano L, Cava C, Garolini D, Sabedot TS, Malta TM, Pagnotta SM, Castiglioni I, Ceccarelli M, Bontempi G, Noushmehr H. TCGAbiolinks: an R/bioconductor package for integrative analysis of TCGA data. Nucleic Acids Res 2016; 44: e71.

14) Yoshihara K, Tsunoda T, Shigemizu D, Fujiwara H, Hatae M, Fujiwara H, Masuzaki H, Katabuchi H, Kawakami Y, Okamoto A, Nogawa T, Matsumura N, Udagawa Y, Saito T, Itamochi H, Takano M, Miyagi E, Sudo T, Ushijima K, Iwase H, Seki H, Terao Y, Enomoto T, Mikami M, Akazawa K, Tsuda H, Moriya T, Tajima A, Inoue I, Tanaka K, Japanese Serous Ovarian Cancer Study Group. High-risk ovarian cancer based on 126-gene expression signature is uniquely characterized by downregulation of antigen presentation pathway. Clin Cancer Res 2012; 18: 1374-1385.

15) Yoshihara K, Shahmoradgoli M, Martínez E, Vegesna R, Kim H, Torres-Garcia W, Treviño V, Shen H, Laird PW, Levine DA, Carter SL, Getz G, Stemke-Hale K, Mills GB, Verhaak RGW. Inferring tumour purity and stromal and immune cell admixture from expression data. Nat Commun 2013; 4: 2612.

16) Langfelder P, Horvath S. WGCNA: an R package for weighted correlation network analysis. BMC Bioinformatics 2008; 9: 559.

17) Jia A, Xu L, Wang Y. Venn diagrams in bioinformatics. Brief Bioinform 2021; 22: bbab108.

18) Chen H, Luo J, Guo J. Development and validation of a five-immune gene prognostic risk model in colon cancer. BMC Cancer 2020; 20: 395.

19) Díaz-Coto S, Corral-Blanco NO, Martínez-Camblor P. Two-stage receiver operating-characteristic curve estimator for cohort studies. Int J Biostat 2020; 17: 117-137.

20) Barbie DA, Tamayo P, Boehm JS, Kim SY, Moody SE, Dunn IF, Schinzel AC, Sandy P, Meylan E, Scholl C, Fröhling S, Chan EM, Sos ML, Michel K, Mermel C, Silver SJ, Weir BA, Reiling JH, Sheng Q, Gupta PB, Wadlow RC, Le H, Hoersch S, Wittner BS, Ramaswamy S, Livingston DM, Sabatini DM, Meyerson M, Thomas RK, Lander ES, Mesirov JP, Root DE, Gilliland DG, Jacks T, Hahn WC. Systematic RNA interference reveals that oncogenic KRAS-driven cancers require TBK1. Nature 2009; 462: 108-112.

21) Mariathasan S, Turley SJ, Nickles D, Castiglioni A, Yuen K, Wang Y, Kadel EE III, Koeppen H, Astarita JL, Cubas R, Jhunjhunwala S, Banchereau R, Yang Y, Guan Y, Chalouni C, Ziai J, Şenbabaoğlu Y, Santoro S, Sheinson D, Hung J, Giltnane JM, Pierce AA, Mesh K, Lianoglou S, Riegler J, Carano RAD, Eriksson P, Höglund M, Somarriba L, Halligan DL, van der Heijden MS, Loriot Y, Rosenberg JE, Fong L, Mellman I, Chen DS, Green M, Derleth C, Fine GD, Hegde PS, Bourgon R, Powles T. TGFβ attenuates tumour response to PD-L1 blockade by contributing to exclusion of T cells. Nature 2018; 554: 544-548.

22) Jiang P, Gu S, Pan D, Fu J, Sahu A, Hu X, Li Z, Traugh N, Bu X, Li B, Liu J, Freeman GJ, Brown MA, Wucherpfennig KW, Liu XS. Signatures of T cell dysfunction and exclusion predict cancer immunotherapy response. Nat Med 2018; 24: 1550-1558.

23) Zhang Y, Hong YK, Zhuang DW, He XJ, Lin ME. Bladder cancer survival nomogram: development and validation of a prediction tool, using the SEER and TCGA databases. Medicine (Baltimore) 2019; 98: e17725.

24) Schneider D, Halperin R, Halperin D, Bukovsky I, Hadas E. Prediction of the survival of patients with advanced ovarian cancer according to a risk model based on a scoring system. Eur J Gynaecol Oncol 1998; 19: 547-552.

25) Yang R, Xiong J, Deng D, Wang Y, Liu H, Jiang G, Peng Y, Peng X, Zeng X. An integrated model of clinical information and gene expression for prediction of survival in ovarian cancer patients. Transl Res 2016; 172: 84-95.

26) Wang Y, Lei L, Chi YG, Liu LB, Yang BP. A comprehensive understanding of ovarian carcinoma survival prognosis by novel biomarkers. Eur Rev Med Pharmacol Sci 2019; 23: 8257-8264.

27) Hwang WT, Adams SF, Tahirovic E, Hagemann IS, Coukos G. Prognostic significance of tumor-infiltrating T cells in ovarian cancer: a meta-analysis. Gynecol Oncol 2012; 124: 192-198.

28) Yang J, Hong S, Zhang X, Liu J, Wang Y, Wang Z, Gao L, Hong L. Tumor immune microenvironment related gene-based model to predict prognosis and response to compounds in ovarian cancer. Front Oncol 2021; 11: 807410.

29) Wang H, Wu X, Chen Y. Stromal-immune score-based gene signature: a prognosis stratification tool in gastric cancer. Front Oncol 2019; 9: 1212.

30) Ma Q, Chen Y, Xiao F, Hao Y, Song Z, Zhang J, Okuda K, Um SW, Silva M, Shimada Y, Si C, Liang C. A signature of estimate-stromal-immune score-based genes associated with the prognosis of lung adenocarcinoma. Transl Lung Cancer Res 2021; 10: 1484-1500.

31) Jia J, Dai Y, Zhang Q, Tang P, Fu Q, Xiong G. Stromal score-based gene signature: a prognostic prediction model for colon cancer. Front Genet 2021; 12: 655855.

32) Xu Y, Xu Y, Wang C, Xia B, Mu Q, Luan S, Fan J. Mining TCGA database for gene expression in ovarian serous cystadenocarcinoma microenvironment. PeerJ 2021; 9: e11375.

33) Chen Y, Meng Z, Zhang L, Liu F. CD2 Is a novel immune-related prognostic biomarker of invasive breast carcinoma that modulates the tumor microenvironment. Front Immunol 2021; 12: 664845.

34) Demetriou P, Abu-Shah E, Valvo S, McCuaig S, Mayya V, Kvalvaag A, Starkey T, Korobchevskaya K, Lee LYW, Friedrich M, Mann E, Kutuzov MA, Morotti M, Wietek N, Rada H, Yusuf S, Afrose J, Siokis A, Meyer-Hermann M, Ahmed AA, Depoil D, Dustin ML. A dynamic CD2-rich compartment at the outer edge of the immunological synapse boosts and integrates signals. Nat Immunol 2020; 21: 1232-1243.

35) McNerney ME, Kumar V. The CD2 family of natural killer cell receptors. Curr Top Microbiol Immunol 2006; 298: 91-120.

36) Qin Y, Liu H, Huang X, Huang L, Liao L, Li J, Zhang L, Li W, Yang J. GIMAP7 as a potential predictive marker for pan-cancer prognosis and immunotherapy efficacy. J Inflamm Res 2022; 15: 1047-1061.

37) Schwefel D, Arasu BS, Marino SF, Lamprecht B, Köchert K, Rosenbaum E, Eichhorst J, Wiesner B, Behlke J, Rocks O, Mathas S, Daumke O. Structural insights into the mechanism of GTPase activation in the GIMAP family. Structure 2013; 21: 550-559.

38) Chien J, Campioni M, Shridhar V, Baldi A. HtrA serine proteases as potential therapeutic targets in cancer. Curr Cancer Drug Targets 2009; 9: 451-468.

39) Kim S, Han Y, Kim SI, Lee J, Jo H, Wang W, Cho U, Park WY, Rando TA, Dhanasekaran DN, Song YS. Computational modeling of malignant ascites reveals CCL5–SDC4 interaction in the immune microenvironment of ovarian cancer. Mol Carcinog 2021; 60: 297-312.

40) James NE, Miller K, LaFranzo N, Lips E, Woodman M, Ou J, Ribeiro JR. Immune modeling analysis reveals immunologic signatures associated with improved outcomes in high grade serous ovarian cancer. Front Oncol 2021; 11: 622182.

41) Qiu X, Klausen C, Cheng JC, Leung PC. CD40 ligand induces RIP1-dependent, necroptosis-like cell death in low-grade serous but not serous borderline ovarian tumor cells. Cell Death Dis 2015; 6: e1864.

42) Guy CS, Vignali DA. Organization of proximal signal initiation at the TCR: CD3 complex. Immunol Rev 2009; 232: 7-21.

43) Landi D, Gemignani F, Barale R, Landi S. A catalog of polymorphisms falling in microRNA-binding regions of cancer genes. DNA Cell Biol 2008; 27: 35-43.

44) Yin J, Fu W, Dai L, Jiang Z, Liao H, Chen W, Pan L, Zhao J. ANKRD22 promotes progression of non-small cell lung cancer through transcriptional up-regulation of E2F1. Sci Rep 2017; 7: 4430.

45) Qiu Y, Yang S, Pan T, Yu L, Liu J, Zhu Y, Wang H. ANKRD22 is involved in the progression of prostate cancer. Oncol Lett 2019; 18: 4106-4113.

46) Lisio MA, Fu L, Goyeneche A, Gao ZH, Telleria C. High-grade serous ovarian cancer:basic sciences, clinical and therapeutic standpoints. Int J Mol Sci 2019; 20: 952.

47) Chen DS, Mellman I. Oncology meets immunology: the cancer-immunity cycle. Immunity 2013; 39: 1-10.

48) Zhang H, Wu Y, Li H, Sun L, Meng X. Model constructions of chemosensitivity and prognosis of high grade serous ovarian cancer based on evaluation of immune microenvironment and immune response. Cancer Cell Int 2021; 21: 593.

49) Li J, Zang XY, Dai Z. Comparative clinical outcomes and predictive biomarkers of sintilimab combinations vs. single therapy in cancer: a systematic review and meta-analysis of randomized controlled trials. Eur Rev Med Pharmacol Sci 2023; 27: 911-923.

50) Liu Y, Liang X, Dong W, Fang Y, Lv J, Zhang T, Fiskesund R, Xie J, Liu J, Yin X, Jin X, Chen D, Tang K, Ma J, Zhang H, Yu J, Yan J, Liang H, Mo S, Cheng F, Zhou Y, Zhang H, Wang J, Li J, Chen Y, Cui B, Hu ZW, Cao X, Xiao-Feng Qin F, Huang B. Tumor-repopulating cells induce PD-1 expression in CD8+ T cells by transferring kynurenine and AhR activation. Cancer Cell 2018; 33: 480-494.

51) Wang Z, Sun K, Xiao Y, Feng B, Mikule K, Ma X, Feng N, Vellano CP, Federico L, Marszalek JR, Mills GB, Hanke J, Ramaswamy S, Wang J. Niraparib activates interferon signaling and potentiates anti-PD-1 antibody efficacy in tumor models. Sci Rep 2019; 9: 1853.